



# A comprehensive study on the synthesis and paramagnetic properties of PEG-coated $\text{Fe}_3\text{O}_4$ nanoparticles



Jinghai Yang<sup>a,b</sup>, Ping Zou<sup>a,b</sup>, Lili Yang<sup>a,b,\*</sup>, Jian Cao<sup>a,b</sup>, Yunfei Sun<sup>a,b</sup>, Donglai Han<sup>c,d</sup>, Shuo Yang<sup>c,d</sup>, Zhe Wang<sup>a,b</sup>, Gang Chen<sup>a,b</sup>, Bingji Wang<sup>a,b</sup>, Xiangwang Kong<sup>a,b</sup>

<sup>a</sup> Institute of Condensed State Physics, Jilin Normal University, Siping 136000, China

<sup>b</sup> Key Laboratory of Functional Materials Physics and Chemistry of the Ministry of Education, Jilin Normal University, Siping 136000, Jilin, China

<sup>c</sup> State Key Laboratory of Luminescence and Applications, Changchun Institute of Optics, Fine Mechanics and Physics, Chinese Academy of Sciences, Changchun 130033, China

<sup>d</sup> University of Chinese Academy of Sciences, Beijing 100049, China

## ARTICLE INFO

### Article history:

Received 17 October 2013

Received in revised form 24 February 2014

Accepted 3 March 2014

Available online 11 March 2014

### Keywords:

$\text{Fe}_3\text{O}_4$  nanoparticles  
Polyethylene glycol  
Magnetic properties

## ABSTRACT

The PEG-coated  $\text{Fe}_3\text{O}_4$  ( $\text{PEG}-\text{Fe}_3\text{O}_4$ ) nanoparticles had been fabricated through chemical coprecipitation method. We comprehensively investigated the influence of different reaction conditions, such as vapor pressures with opening or sealing the beaker, molecular weights and amounts of PEG, on the structural and paramagnetic properties of  $\text{PEG}-\text{Fe}_3\text{O}_4$  nanoparticles. The well-dispersed magnetic  $\text{PEG}-\text{Fe}_3\text{O}_4$  nanoparticles with better size distribution can be obtained with adding 4 g PEG1000 while sealing the beaker. The possible growth mechanism was also discussed in detail.

© 2014 Elsevier B.V. All rights reserved.

## 1. Introduction

During last decade, magnetic materials attract lots of interest due to their specific applications, such as drug delivery and biosensing [1], tissue repair [2], detoxification of biological fluids [3] and magnetic resonance imaging [4,5]. Among magnetic nanoparticles (NPs), the magnetite ( $\text{Fe}_3\text{O}_4$ ) and maghemite ( $\gamma\text{-Fe}_2\text{O}_3$ ) are superior to others in the biological application due to their advantages, such as biocompatibility, special magnetic properties and low toxicity [6–10]. However, if the magnetite NPs are absent of some special bio-treatment before application, they might bring poisonous effects on the human body. For example, once the iron ions have been implicated in the generation of reactive oxygen species (ROS), they can cause direct damage to DNA, proteins or lipid molecules [11–14]. Therefore, people usually use some surfactants or biocompatible polymer molecules (e.g., sodium bis(2-ethylhexyl) sulfosuccinate, dextran, etc.) to modify the magnetite NPs to improve their colloidal stability in physiological medium and reduce toxicity [15,16]. Thereinto, polyethylene glycol (PEG) is a popular one since their long polymeric chains are highly

soluble in water and nontoxic in the blood. However, so far, nearly all the magnetic  $\text{Fe}_3\text{O}_4$  nanoparticles modified by PEG ( $\text{PEG}-\text{Fe}_3\text{O}_4$ ) were fabricated by sol-gel [17], colloidal [18], pyrolysis reaction [19] or hydrothermal method [20], which usually needs strict atmospheric conditions or higher temperature. For instance, Cheng et al. synthesized well-defined  $\text{PEG}-\text{Fe}_3\text{O}_4$  NPs under the temperature of 200 °C [21]. Hong et al. used stringent reaction condition of Ar atmosphere to synthesize  $\text{PEG}-\text{Fe}_3\text{O}_4$  NPs [22]. Therefore, the synthesis of  $\text{PEG}-\text{Fe}_3\text{O}_4$  NPs with a simple way is very important to prompt their application.

In this work,  $\text{PEG}-\text{Fe}_3\text{O}_4$  NPs were synthesized via a simple coprecipitation route at 60 °C under different external condition, such as vapor pressures with opening or sealing the beaker, molecular weights of PEG or amounts of PEG, in order to obtain better size distribution and magnetic property. The corresponding influence mechanisms were also discussed in detail.

## 2. Experiments

All chemicals (analytical grade reagents) were directly used without further purification. All the samples were synthesized at 60 °C with a coprecipitation reaction route. For pure  $\text{Fe}_3\text{O}_4$  NPs, the  $\text{FeCl}_2 \cdot 4\text{H}_2\text{O}$  and  $\text{FeCl}_3 \cdot 6\text{H}_2\text{O}$  were firstly dissolved in deionized water with 1:2 molar ratios. The obtained dark orange solution was stirred for 5 min. Then an aqueous  $\text{NH}_3 \cdot \text{H}_2\text{O}$  solution (25%) was

\* Corresponding author at: Institute of Condensed State Physics, Jilin Normal University, Siping 136000, China. Tel.: +86 434 3294566; fax: +86 434 3294566.

E-mail address: [llyang@jlnu.edu.cn](mailto:llyang@jlnu.edu.cn) (L. Yang).

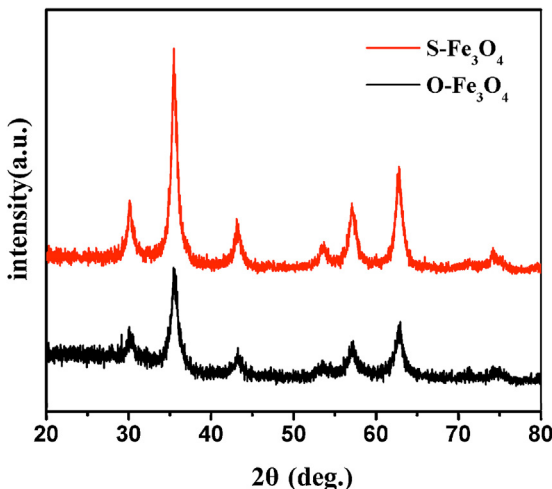


**Fig. 1.** XRD patterns of O-Fe<sub>3</sub>O<sub>4</sub> and S-Fe<sub>3</sub>O<sub>4</sub> NPs.

added dropwise to the above solution at 60 °C. After 40 min reaction, the color of the solution changed from dark orange to black, indicating the formation of Fe<sub>3</sub>O<sub>4</sub> NPs. After cooling to room temperature, the Fe<sub>3</sub>O<sub>4</sub> NPs were separated and purified by magnetic separation and washed with deionized water and ethanol several times to make them free of any residual salts, and then dried in a vacuum at 60 °C for 24 h. The sample grown in the open beaker is named O-Fe<sub>3</sub>O<sub>4</sub>; the other grown in the sealed beaker is named S-Fe<sub>3</sub>O<sub>4</sub>. For the PEG-Fe<sub>3</sub>O<sub>4</sub> NPs, FeCl<sub>2</sub>·4H<sub>2</sub>O and FeCl<sub>3</sub>·6H<sub>2</sub>O with a molar ratio of 1:2 were mixed together with 30 mL of deionized water. Then the PEG with different molecular weights (PEG400, PEG1000 and PEG2000) was added into it respectively to form a stable orange solution. We also tried to add different amounts (4 g, 8 g, 10 g) of PEG1000 to prepare the Fe<sub>3</sub>O<sub>4</sub> NPs. All the other experimental conditions are identical as that of pure Fe<sub>3</sub>O<sub>4</sub> NPs. The PEG-Fe<sub>3</sub>O<sub>4</sub> NPs grown in the open beaker is named O-PEG-Fe<sub>3</sub>O<sub>4</sub>; the other grown in the sealed beaker is named S-PEG-Fe<sub>3</sub>O<sub>4</sub>.

X-ray diffraction (XRD) patterns were recorded by a MAC Science MXP-18 X-ray diffractometer using a Cu target radiation source. Scanning electron microscopy (SEM) pictures were collected on a Hitachi, S-570 SEM. Transmission electron micrographs (TEM) and high-resolution TEM (HRTEM) images were taken on JEM-2100 transmission electron microscope. A quantitative compositional analysis was carried out by using an X-ray photoelectron spectroscopy (XPS) in an ultra-high vacuum chamber at a pressure lower than 1.333 × 10<sup>-7</sup> Pa. The magnetic properties of the samples were measured by a Lake Shore 7407 vibrating sample magnetometry (VSM).

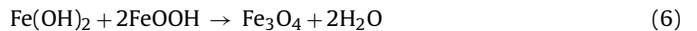
### 3. Results and discussion

#### 3.1. Effects of open or sealed environment

The XRD patterns of the as-grown O-Fe<sub>3</sub>O<sub>4</sub> and S-Fe<sub>3</sub>O<sub>4</sub> NPs by chemical coprecipitation method are shown in Fig. 1. All the observed diffraction peaks can be indexed to Fe<sub>3</sub>O<sub>4</sub> with face-centered cubic structure according to JCPDS card No. 19-0629 [23], which indicates no other impurity phase exists in the samples. We also observe in Fig. 1 that, the full width at half maximum (FWHM) of diffraction peaks for S-Fe<sub>3</sub>O<sub>4</sub> is narrower than that of O-Fe<sub>3</sub>O<sub>4</sub>, indicating a better crystallinity of S-Fe<sub>3</sub>O<sub>4</sub>. The average crystalline size has been calculated using the Scherrer equation:

$$D = \frac{0.89\lambda}{\beta \cos \theta} \quad (1)$$

where  $D$  (in nm) is the size of the nanocrystal,  $\lambda$  is the wavelength (in nm) emitted by the X-ray source ( $\lambda = 0.154178$  nm in our experiment),  $2\theta$  is the angle at which the peak is observed, and  $\beta$  (in radian) is the FWHM of the diffraction peaks. According to the Eq. (1), the calculated average crystalline size of O-Fe<sub>3</sub>O<sub>4</sub> and S-Fe<sub>3</sub>O<sub>4</sub> is 14.5 nm and 15.2 nm, respectively. For S-Fe<sub>3</sub>O<sub>4</sub> samples, the reactions in solution can be described by the following formulas [24]:



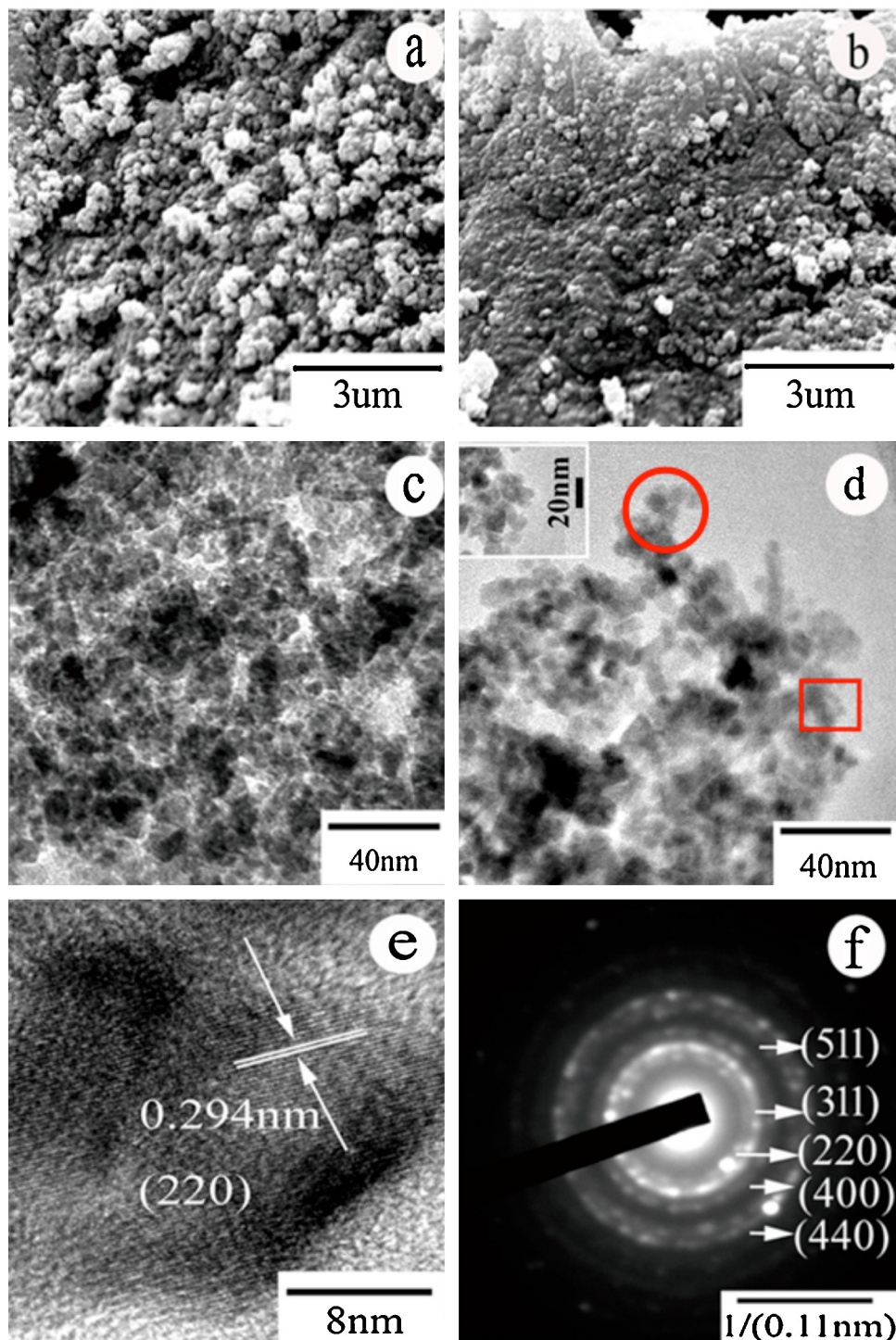
NH<sub>3</sub>·H<sub>2</sub>O, which is extensively used in the fabrication of Fe<sub>3</sub>O<sub>4</sub> NPs, provides the hydroxide ions (OH<sup>-</sup>) and the ammonia molecules (NH<sub>3</sub>) to the solution. Under the open environment, the NH<sub>3</sub> and H<sub>2</sub>O will unceasingly evaporate from the solution during the whole growth process. On the other hand, when the beaker is sealed, all the NH<sub>3</sub> and H<sub>2</sub>O cannot evaporate outside so that the pressure in the beaker increases. Besides, more OH<sup>-</sup> will participate in the growth of Fe<sub>3</sub>O<sub>4</sub> NPs. These two factors result in the faster growth of S-Fe<sub>3</sub>O<sub>4</sub> than O-Fe<sub>3</sub>O<sub>4</sub> NPs, which finally makes the size of S-Fe<sub>3</sub>O<sub>4</sub> bigger than O-Fe<sub>3</sub>O<sub>4</sub> NPs [25,26].

Fig. 2a and b displays the typical SEM images of the as-synthesized O-Fe<sub>3</sub>O<sub>4</sub> and S-Fe<sub>3</sub>O<sub>4</sub> NPs. Through comparison, the aggregation of O-Fe<sub>3</sub>O<sub>4</sub> NPs is more obvious than S-Fe<sub>3</sub>O<sub>4</sub> NPs. We further carried out TEM characterization to reveal the detailed microscopic structure. Fig. 2c and d shows the TEM images of the as-synthesized O-Fe<sub>3</sub>O<sub>4</sub> and S-Fe<sub>3</sub>O<sub>4</sub> NPs, from which we can also observe obvious aggregation of O-Fe<sub>3</sub>O<sub>4</sub> NPs. To see the NPs clearly, the magnified TEM images according to the place marked by the red box can be find the inset of Fig. 2d. Moreover, the HRTEM images corresponding to the place marked by the red ring in the Fig. 2d was shown in Fig. 2e. The fringe space is 0.294 nm, which is corresponding to the (2 2 0) plane distance of the standard Fe<sub>3</sub>O<sub>4</sub> with face-centered cubic structure. The corresponding selected area electron diffraction pattern (SAED) shown in Fig. 2f reveals that the S-Fe<sub>3</sub>O<sub>4</sub> NPs are polycrystalline [27].

To investigate the magnetic properties of O-Fe<sub>3</sub>O<sub>4</sub> and S-Fe<sub>3</sub>O<sub>4</sub> NPs, their hysteresis loops were measured by VSM at room temperature. Fig. 3 shows their magnetization curves. When the magnetic field is cycled between -15,000 and 15,000, zero coercivity for both samples is obtained, which indicates their superparamagnetic properties [28]. Moreover, the saturation magnetization (Ms) for S-Fe<sub>3</sub>O<sub>4</sub> and O-Fe<sub>3</sub>O<sub>4</sub> NPs is 44 emu/g and 24 emu/g, respectively. We would like to point out that the obtained Ms value for both samples are lower than the bulk material (92 emu/g) [29]. This reduction of Ms in magnetite NPs may be attributed to the surface disorder or spin canting at the surface of NPs [30]. Moreover, we know that the size of both samples is almost same, so the difference for the Ms should be related to their crystal quality [31]. In our case, the crystalline quality of S-Fe<sub>3</sub>O<sub>4</sub> NPs is higher than that of O-Fe<sub>3</sub>O<sub>4</sub> NPs as XRD results revealed, therefore, the S-Fe<sub>3</sub>O<sub>4</sub> NPs own larger saturation magnetization.

#### 3.2. Effects of coating PEG

The XRD patterns of pure S-Fe<sub>3</sub>O<sub>4</sub> and S-PEG-Fe<sub>3</sub>O<sub>4</sub> NPs are quite similar to Fig. 1 so that we did not present them here. Interestingly, the average grain size calculated from XRD patterns is approximately 15.1 nm and 15.4 nm, respectively, indicating no significant size change has occurred after the PEG coating. To further



**Fig. 2.** (a) SEM image of O- $\text{Fe}_3\text{O}_4$  NPs; (b) SEM image of S- $\text{Fe}_3\text{O}_4$  NPs; (c) TEM images of O- $\text{Fe}_3\text{O}_4$  NPs; (d) TEM images of S- $\text{Fe}_3\text{O}_4$  NPs; (e) HRTEM image of S- $\text{Fe}_3\text{O}_4$  NPs; (f) SAED image of S- $\text{Fe}_3\text{O}_4$  NPs. (For interpretation of the references to color in this figure legend, the reader is referred to the web version of this article.)

prove it, Fig. 4a and b illustrates the SEM images of S- $\text{Fe}_3\text{O}_4$  and S-PEG- $\text{Fe}_3\text{O}_4$  NPs. Clearly, the grain size of S-PEG- $\text{Fe}_3\text{O}_4$  NPs is similar with that of S- $\text{Fe}_3\text{O}_4$  NPs. The corresponding TEM images are shown in Fig. 4c and d. We can observe that S-PEG- $\text{Fe}_3\text{O}_4$  NPs are mostly spherical with an average size around 15 nm, similar to S- $\text{Fe}_3\text{O}_4$  NPs. Moreover, we can also see that the S-PEG- $\text{Fe}_3\text{O}_4$  NPs

exhibit better dispersion due to the addition of PEG. As we known, there are three types of interaction among these NPs: London-Van der Waals force, magnetic force and repulsive force of the double electronic layer. The previous two affinities among the NPs must be counteracted by the later reacting force to make the NPs exist stably in the solution. But this kind of repulsive force is very small

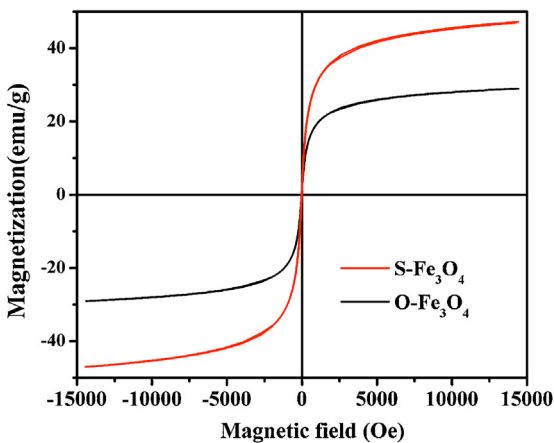


Fig. 3. Magnetic hysteresis loops of O- $\text{Fe}_3\text{O}_4$  and S- $\text{Fe}_3\text{O}_4$  NPs.

[15]. Thus, people usually modify some surfactants on the NPs to make them absorb one layer of surfactant on the surface to make the NPs disperse well in the solution. In our case, PEG owns hydrophilic surfaces, the space hindrance repulsive force can conquer the affinities between  $\text{Fe}_3\text{O}_4$  NPs, which results in a better dispersion of S-PEG- $\text{Fe}_3\text{O}_4$  NPs. The corresponding HRTEM image of S-PEG- $\text{Fe}_3\text{O}_4$  NPs is shown in Fig. 4e. We can clearly see the fringe lines along two directions with fringe spaces of 0.254 nm and 0.294 nm, which was corresponding to the (3 1 1) and (2 2 0) plane distance of the spinel structure, respectively [31]. Moreover, it is worth to note that we can obviously see an amorphous layer covering the  $\text{Fe}_3\text{O}_4$  NPs as marked by red line in Fig. 4e, which indicates PEG layer with 0.375 nm in thickness had successfully deposited on the  $\text{Fe}_3\text{O}_4$  cores. Furthermore, Fig. 4f shows the corresponding SAED image of S-PEG- $\text{Fe}_3\text{O}_4$  NPs, revealing the sample owns the spinel structure with polycrystalline.

To further prove that the PEG has been coated on the  $\text{Fe}_3\text{O}_4$  NPs, we utilize XPS technique to investigate the chemical compositions and the bonding states of the sample. Fig. 5a shows the XPS survey spectra obtained from S-PEG- $\text{Fe}_3\text{O}_4$  and S- $\text{Fe}_3\text{O}_4$  NPs. All peaks can be ascribed to Fe, C, and O elements as labeled in Fig. 5a, which indicates that no other impurities exist in both samples. Fig. 5b shows the Fe 2p XPS spectra of S- $\text{Fe}_3\text{O}_4$  and S-PEG- $\text{Fe}_3\text{O}_4$  NPs. The peaks located at 710.3 eV and 723.7 eV are ascribed to the Fe 2p3/2 and Fe 2p1/2 core level of  $\text{Fe}_3\text{O}_4$  [32]. Usually, the  $\text{Fe}^{3+}$  in  $\text{Fe}_2\text{O}_3$  exhibits a shakeup satellite peak around 719.0 eV. In our case, the absence of this characteristic peak confirms the pure magnetite phase in these samples [31]. Fig. 5c and d shows the high resolution scans of C1s core level of S- $\text{Fe}_3\text{O}_4$  and S-PEG- $\text{Fe}_3\text{O}_4$  NPs. Fig. 5e and f shows the O1s core level lines from S- $\text{Fe}_3\text{O}_4$  and S-PEG- $\text{Fe}_3\text{O}_4$  NPs. For these spectra, the open circles denote the experimental data, the red solid lines represent the fitting curves, and the deconvoluted individual peaks are depicted by green lines. Here we would like to point out that all binding energies have been calibrated by taking the carbon C1s peak (285.0 eV) as reference in Fig. 5c. As shown in Fig. 5d, the deconvolutions of the XPS spectra for core level C1s from S-PEG- $\text{Fe}_3\text{O}_4$  NPs contain four components, indicating four carbon species exist in them: the adventitious carbon at 284.3 eV (C1), the carbon in C-C at 284.8 eV (C2), the carbon in C-OH at 285.7 eV (C3) and the carbon in  $(-\text{CH}_2\text{O}-)_n$  at 288.6 eV (C4). According to the molecular formula of PEG displayed in the inset of Fig. 5f, we believe that the above C2, C3 and C4 species are originated from PEG, indicating the PEG is successfully coated on the  $\text{Fe}_3\text{O}_4$  NPs. In Fig. 5e, the deconvolutions show the presence of three different O1s peaks in the S- $\text{Fe}_3\text{O}_4$  NPs. The peak centered at 529.6 eV is associated to the  $\text{O}^{2-}$  forming oxide with iron (O1). The peak at 531.2 eV is attributed to the presence of OH bonds (O2) [33]. The peak at 532.8 eV can be

ascribed to the specifically chemisorbed oxygen, such as adsorbed  $\text{O}_2$  or  $\text{H}_2\text{O}$  ( $\text{O}_3$ ) [25]. However, for S-PEG- $\text{Fe}_3\text{O}_4$  NPs, except the above three oxygen species, we can see another peak located at 533.4 eV, which is related to the C-O bonds (O4) [33], indicating the existence of PEG in the sample and further testifying the results of C 1s XPS spectra. Moreover, in comparison with Fig. 5e, the locations of O1, O2 and O3 peaks exhibit more or less change, which is mainly caused by the PEG coating.

Fig. 6 shows the magnetization curves of S- $\text{Fe}_3\text{O}_4$  and S-PEG- $\text{Fe}_3\text{O}_4$  NPs. No hysteresis loop is observed for both samples, indicating a superparamagnetic behavior. In addition, we can also see that the  $M_s$  decreases from 77 emu/g for S- $\text{Fe}_3\text{O}_4$  NPs to 35.3 emu/g for S-PEG- $\text{Fe}_3\text{O}_4$  NPs due to the PEG coating. It is known that the change of size and surface state in  $\text{Fe}_3\text{O}_4$  NPs will greatly affect magnetic properties [16]. No significant size change has occurred due to PEG coating as revealed in the previous sections, therefore, the changes in the magnetic properties can be attributed to the surface modifications by PEG polymer molecules.

We further prepare the PEG- $\text{Fe}_3\text{O}_4$  NPs in the open environment (named O-PEG- $\text{Fe}_3\text{O}_4$ ). The XRD and VSM spectra of S-PEG- $\text{Fe}_3\text{O}_4$  and O-PEG- $\text{Fe}_3\text{O}_4$  NPs are presented in Fig. 7a and b. Through comparison, we find that the grain size of both samples are all about 15 nm and the  $M_s$  of S-PEG- $\text{Fe}_3\text{O}_4$  NPs is higher than that of O-PEG- $\text{Fe}_3\text{O}_4$  NPs, which further testifies the results of Figs. 1 and 3.

### 3.3. Effects of molecular weights and amounts of PEG

It is known that smaller  $\text{Fe}_3\text{O}_4$  NPs have larger specific surface area, which causes intermolecular aggregation. The above discussion reveals that PEG coating can effectively prompt the dispersion of  $\text{Fe}_3\text{O}_4$  NPs. To obtain the optimized growth condition, we further prepare the S-PEG- $\text{Fe}_3\text{O}_4$  NPs with different molecular weights (400, 1000 and 2000) and with adding different amount of PEG1000 (4 g, 8 g and 10 g). Since the XRD patterns (Fig. 8a) of samples are all similar with the previous XRD results, we will only discuss the magnetic properties of S-PEG- $\text{Fe}_3\text{O}_4$  NPs in the following sections. Fig. 8b presents the magnetization curves for S-PEG400- $\text{Fe}_3\text{O}_4$ , S-PEG1000- $\text{Fe}_3\text{O}_4$  and S-PEG2000- $\text{Fe}_3\text{O}_4$  NPs. No hysteresis loops are observed for three samples, indicating their superparamagnetic behaviors. The corresponding  $M_s$  is 72 emu/g, 57 emu/g, and 23 emu/g for S-PEG400- $\text{Fe}_3\text{O}_4$ , S-PEG1000- $\text{Fe}_3\text{O}_4$  and S-PEG2000- $\text{Fe}_3\text{O}_4$  respectively. It was found that the  $M_s$  decreased with increasing the molecular weight (400, 1000, 2000) of PEG. As Ren et al. reported, the polymers with larger molecular weight can make better conjunction to  $\text{Fe}_3\text{O}_4$  NPs, lead to well-enwrapped large particles, which make the decrease of magnetic property more remarkable [34].

Fig. 8c shows the XRD patterns of S-PEG1000- $\text{Fe}_3\text{O}_4$ -4 g, S-PEG1000- $\text{Fe}_3\text{O}_4$ -8 g and S-PEG1000- $\text{Fe}_3\text{O}_4$ -10 g NPs, wherein all of the XRD peaks can be indexed to the  $\text{Fe}_3\text{O}_4$  with face-centered-cubic phase (JCPDS no.19-0629) [23]. No significant size change has occurred with adding different amounts of PEG1000 (4 g, 8 g and 10 g). The calculated average crystalline size of S-PEG1000- $\text{Fe}_3\text{O}_4$ -4 g, S-PEG1000- $\text{Fe}_3\text{O}_4$ -8 g and S-PEG1000- $\text{Fe}_3\text{O}_4$ -10 g NPs is 15 nm and 15.2 nm, 15.5 nm, respectively by using the Debye-Scherrer equation. The VSM curves of obtained powders are presented in Fig. 8d. Clearly, with increasing the amounts of PEG1000, the  $M_s$  decreases step by step, since usually the more nonmagnetic component per gram of a sample, the lower mass content of  $\text{Fe}_3\text{O}_4$  NPs as the mass of the PEG increased [35].

### 3.4. Effects of stability by coating PEG

Usually, the  $\text{Fe}_3\text{O}_4$  is apt to transform to  $\text{Fe}_2\text{O}_3$  after certain time in the air. To see the stability of S-PEG1000- $\text{Fe}_3\text{O}_4$ -4 g, we

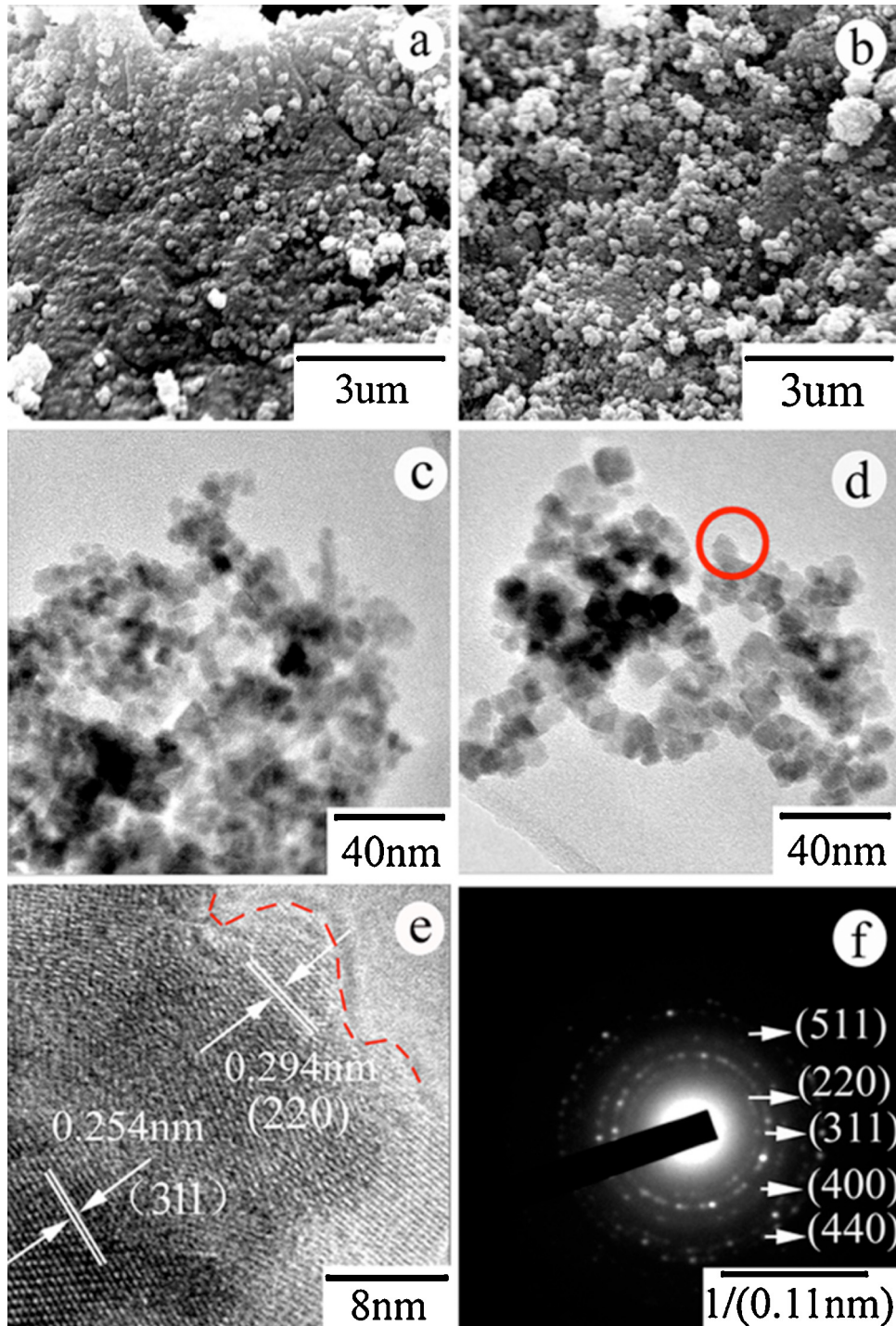


**Fig. 4.** (a) SEM image of S- $\text{Fe}_3\text{O}_4$  NPs; (b) SEM image of S-PEG- $\text{Fe}_3\text{O}_4$  NPs; (c) TEM image of S- $\text{Fe}_3\text{O}_4$  NPs; (d) TEM image of S-PEG- $\text{Fe}_3\text{O}_4$  NPs; (e) HRTEM image of S-PEG- $\text{Fe}_3\text{O}_4$  NPs corresponding to the region marked by the red dot ring in (d) and (f) SAED image of the S-PEG- $\text{Fe}_3\text{O}_4$  NPs. (For interpretation of the references to color in this figure legend, the reader is referred to the web version of this article.)

repeated the measurements of XRD and XPS spectra after 1 month. For the as grown sample and 1 month sample, we named them as A and A-1 respectively. Their XRD patterns are shown in Fig. 9a. We can see that all the diffraction peaks can be indexed to  $\text{Fe}_3\text{O}_4$  according to JCPDS card No. 19-0629 [23], which indicates that PEG can effectively prevent the  $\text{Fe}_3\text{O}_4$  from being

oxidized. Fig. 9b shows their Fe2p XPS spectra. For both samples, the peaks located at about 710.3 eV and 723.7 eV are ascribed to the Fe 2p3/2 and Fe 2p1/2 core level of  $\text{Fe}_3\text{O}_4$ . Moreover, the absence of shakeup satellite peak confirms that they are  $\text{Fe}_3\text{O}_4$ , which illustrated that the  $\text{Fe}_3\text{O}_4$  NPs with PEG coating have good stability.

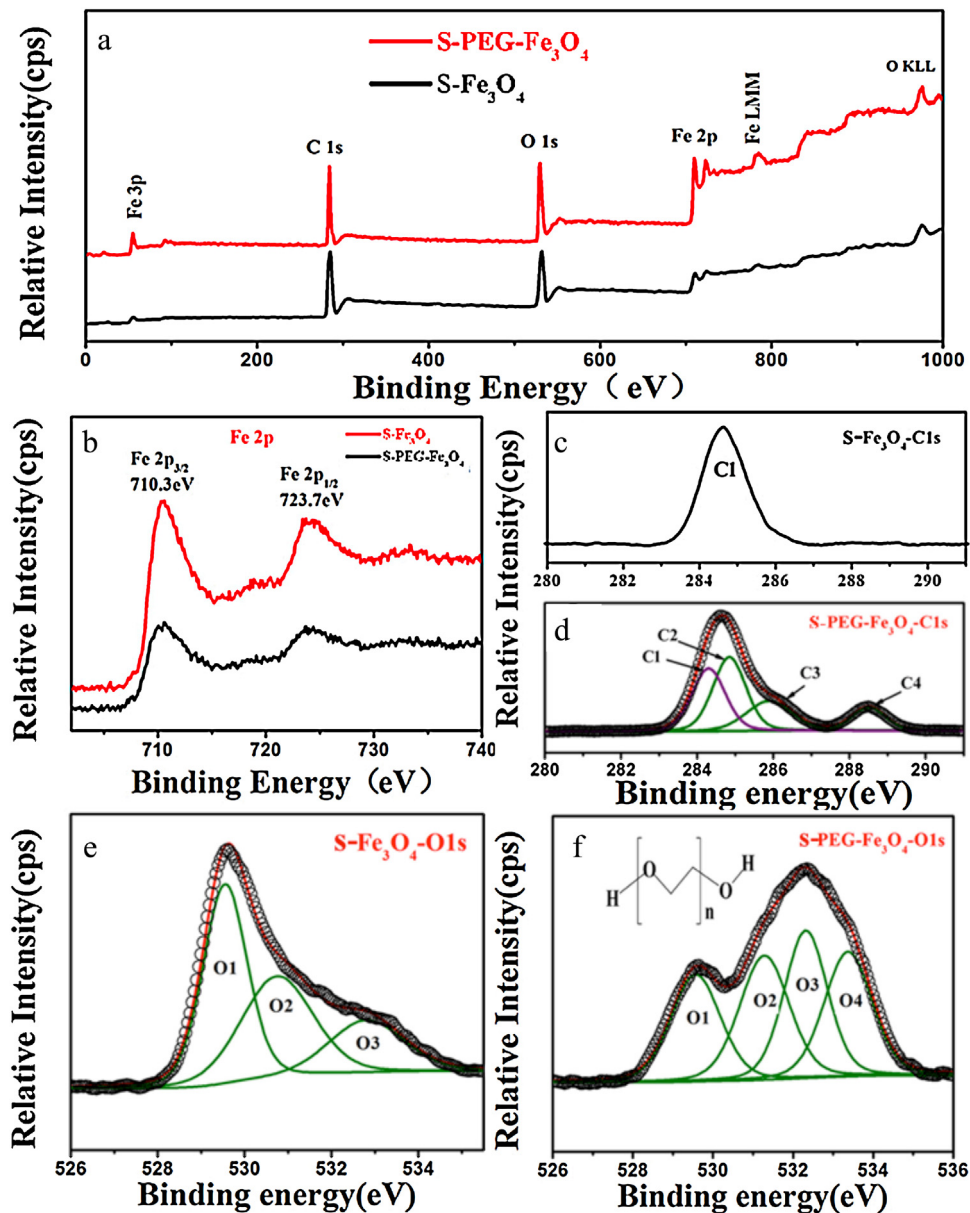


**Fig. 5.** XPS spectrum of S-Fe<sub>3</sub>O<sub>4</sub> NPs and S-PEG-Fe<sub>3</sub>O<sub>4</sub> NPs. (a) XPS survey spectrum; (b) Fe 2p XPS spectrum; (c) C1s XPS spectrum of S-Fe<sub>3</sub>O<sub>4</sub> NPs. (d) C1s XPS spectrum of S-PEG-Fe<sub>3</sub>O<sub>4</sub> NPs; (e) O1s XPS spectrum of S-Fe<sub>3</sub>O<sub>4</sub> NPs and (f) O1s XPS spectrum of S-PEG-Fe<sub>3</sub>O<sub>4</sub> NPs. The inset is the molecular formula of PEG.

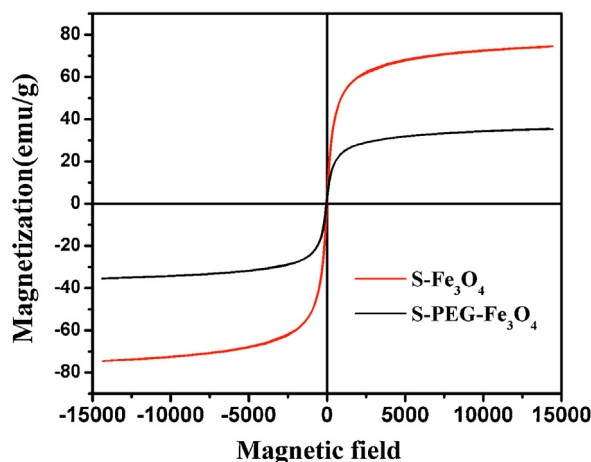


**Fig. 6.** Magnetic hysteresis loops of the S-Fe<sub>3</sub>O<sub>4</sub> NPs and S-PEG-Fe<sub>3</sub>O<sub>4</sub> NPs.

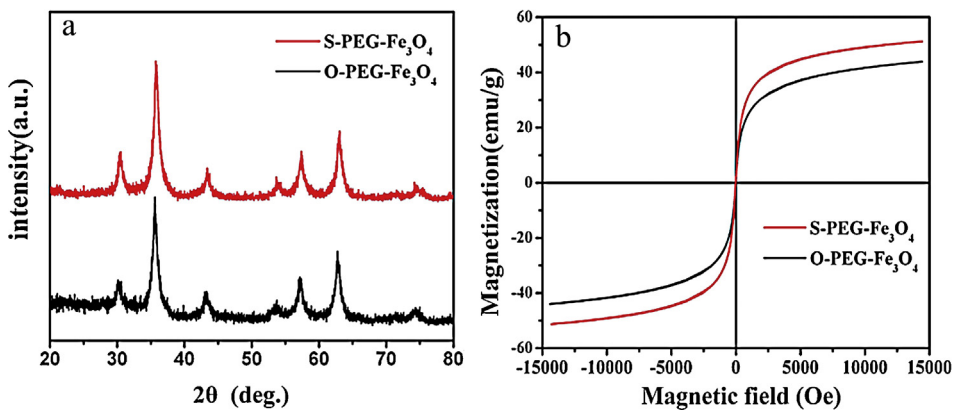


**Fig. 7.** XRD patterns (a) and the magnetic hysteresis loops (b) of O-PEG- $\text{Fe}_3\text{O}_4$  and S-PEG- $\text{Fe}_3\text{O}_4$  NPs.

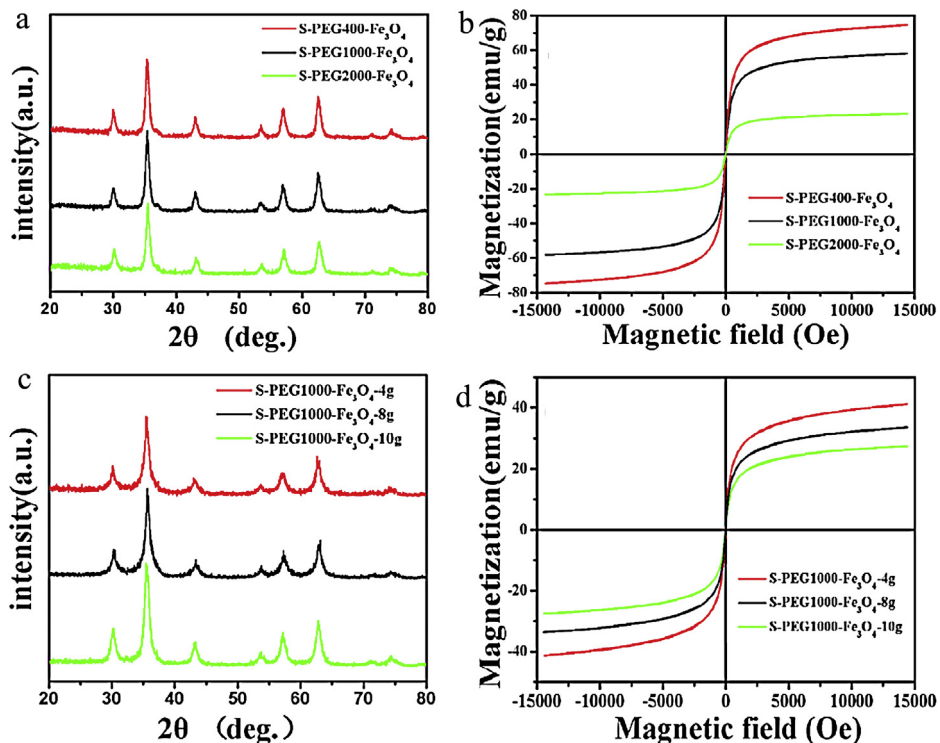


**Fig. 8.** XRD patterns (a) and the magnetic hysteresis loops (b) of S-PEG- $\text{Fe}_3\text{O}_4$  NPs with different PEG molecular weight (400, 1000 and 2000); XRD patterns (c) and the magnetic hysteresis loops (d) of S-PEG1000- $\text{Fe}_3\text{O}_4$  NPs with adding 4 g, 8 g and 10 g PEG1000.

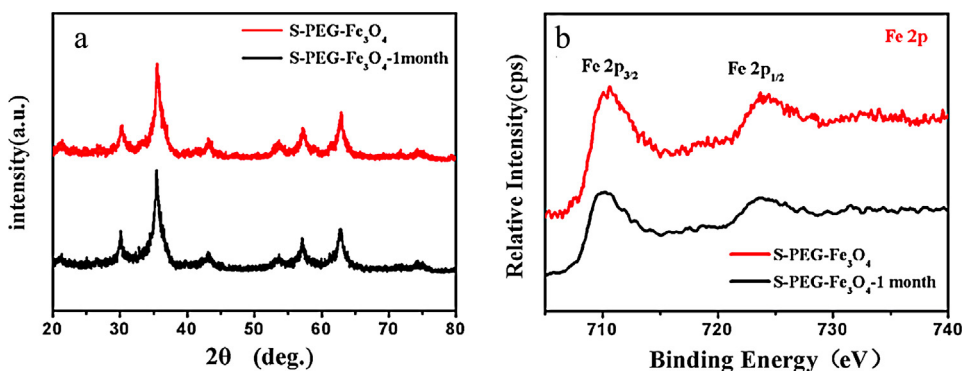


**Fig. 9.** XRD patterns (a) and Fe 2p XPS spectra (b) of A and A-1 samples.

## 4. Conclusions

In this work, we successfully synthesized the PEG-Fe<sub>3</sub>O<sub>4</sub> NPs by a chemical coprecipitation method. The well-dispersed magnetic PEG-Fe<sub>3</sub>O<sub>4</sub> NPs with better size distribution can be obtained with adding 4 g PEG 1000. This method exhibits great advantages, such as low cost and simple operation process, which is appropriate to fabricate biocompatible and surface-modified nanoparticles. Therefore, this work may prompt the tremendous utility of PEG-Fe<sub>3</sub>O<sub>4</sub> NPs in biomedical fields including bioseparation, drug targeting and diagnostic analysis.

## Acknowledgements

The authors would like to acknowledge financial support for this work from National Programs for High Technology Research and Development of China (Item No. 2013AA032202), National Natural Science Foundation of China (Grant Nos. 61178074, 61008051, 11204104, 61308095, 61378085 and 11254001), Program for the Development of Science and Technology of Jilin Province (Item Nos. 201205078, 20110415, and 201115219), Twentieth Five-Year Program for Science and Technology of Education Department of Jilin Province (Item No. 20140147).

## References

- [1] X.F. Zhang, L. Clime, H.Q. Ly, M. Trudeau, T. Veres, Multifunctional Fe<sub>3</sub>O<sub>4</sub>-Au/porous silica@fluorescein core/shell nanoparticles with enhanced fluorescence quantum yield, *J. Phys. Chem. C* 114 (2010) 18313–18317.
- [2] M. Babic, D. Horák, M. Trchová, P. Jendelová, K. Glogarová, P. Lesný, V. Herynek, M. Hájek, E. Syková, Poly(L-lysine)-modified iron oxide nanoparticles for stem cell labeling, *Bioconjug. Chem.* 19 (2008) 740–750.
- [3] A.K. Gupta, M. Gupta, Synthesis and surface engineering of iron oxide nanoparticles for biomedical applications, *Biomaterials* 26 (2005) 3995–4021.
- [4] Z.L. Chen, Y. Sun, P. Huang, X.X. Yang, X.P. Zhou, Studies on preparation of photosensitizer loaded magnetic silica nanoparticles and their anti-tumor effects for targeting photodynamic therapy, *Nanoscale Res. Lett.* 4 (2009) 400–408.
- [5] Y.B. Zhao, Z.M. Qiu, J.Y. Huang, Preparation and analysis of Fe<sub>3</sub>O<sub>4</sub> magnetic nanoparticles used as targeted-drug carriers, *J. Chem. Eng.* 16 (2008) 451–455.
- [6] Y.H. Deng, D. Qi, C.H. Deng, X.M. Zhang, D.Y. Zhao, Superparamagnetic high-magnetization microspheres with an Fe<sub>3</sub>O<sub>4</sub>@SiO<sub>2</sub> core and perpendicularly aligned mesoporous SiO<sub>2</sub> shell for removal of microcystins, *J. Am. Chem. Soc.* 130 (2008) 28–29.
- [7] X. Xu, C. Deng, M. Gao, W. Yu, P. Yang, X. Zhang, Synthesis of magnetic microspheres with immobilized metal ions for enrichment and direct determination of phosphopeptides by matrix-assisted laser desorption ionization mass spectrometry, *Adv. Mater.* 18 (2006) 3289–3293.
- [8] J. Park, K. An, Y. Hwang, J.G. Park, H.J. Noh, J.Y. Kim, J.H. Park, N.M. Hwang, T. Hyeon, Ultra-large-scale syntheses of monodisperse nanocrystals, *Nat. Mater.* 3 (2004) 891–895.
- [9] K. Mori, Y. Kondo, S. Morimoto, H. Yamashita, Synthesis and multifunctional properties of superparamagnetic iron oxide nanoparticles coated with mesoporous silica involving single-site Ti-oxide moiety, *J. Phys. Chem. C* 112 (2008) 397–404.
- [10] A. Zhu, L.H. Yuan, S. Dai, Preparation of well-dispersed superparamagnetic iron oxide nanoparticles in aqueous solution with biocompatible N-succinyl-O-carboxymethylchitosan, *J. Phys. Chem. C* 112 (2008) 5432–5438.
- [11] S. Naqvi, M. Samim, M.Z. Abdin, F.J. Ahmed, A.N. Maitra, C.K. Prashant, A.K. Dinda, Concentration-dependent toxicity of iron oxide nanoparticles mediated by increased oxidative stress, *Int. J. Nanomed.* 5 (2010) 983–989.
- [12] S. Toyokuni, Iron-induced carcinogenesis: the role of redox regulation, *Free Radic. Biol. Med.* 20 (1996) 553–566.
- [13] S. Toyokuni, Iron and carcinogenesis: from fenton reaction to target genes, *Redox Rep.* 7 (2002) 189–197.
- [14] M. Valko, D. Leibfritz, J. Moncol, M.T. Cronin, M. Mazur, J. Telser, Free radicals and antioxidants in normal physiological functions and human disease, *Int. J. Biochem. Cell Biol.* 39 (2007) 44–84.
- [15] H. Yan, J.C. Zhang, C.X. You, Z.W. Song, B.W. Yu, Y. Shen, Influences of different synthesis conditions on properties of Fe<sub>3</sub>O<sub>4</sub> nanoparticles, *Mater. Chem. Phys.* 113 (2009) 46–52.
- [16] A. Mukhopadhyay, N. Joshi, K. Chattopadhyay, G. De, A facile synthesis of PEG-coated magnetite (Fe<sub>3</sub>O<sub>4</sub>) nanoparticles and their prevention of the reduction of cytochrome C, *ACS Appl. Mater. Interfaces* 4 (2012) 142–149.
- [17] J.C. Aphsteguy, S.E. Jacobo, N.N. Schegoleva, G.V. Kurlyandskaya, Characterization of nanosized spinel ferrite powders synthesized by coprecipitation and autocombustion method, *J. Alloys Compd.* 495 (2010) 509–512.
- [18] I. Martínez-Mera, M.E. Espinosa-Pesqueira, R. Pérez-Hernández, J. Arenas-Alatorre, Synthesis of magnetite (Fe<sub>3</sub>O<sub>4</sub>) nanoparticles without surfactants at room temperature, *Mater. Lett.* 61 (2007) 4447–4451.
- [19] W.S. Chiu, S. Radiman, M.H. Abdullah, P.S. Khiew, N.M. Huang, R. Abd-Shukor, One pot synthesis of monodisperse Fe<sub>3</sub>O<sub>4</sub> nanocrystals by pyrolysis reaction of organometallic compound, *Mater. Chem. Phys.* 106 (2007) 231–235.
- [20] P. Sun, H.Y. Zhang, C. Liu, J. Fang, M. Wang, J. Chen, J.P. Zhang, C.B. Mao, S.K. Xu, Preparation and characterization of Fe<sub>3</sub>O<sub>4</sub>/CdTe magnetic/fluorescent nanocomposites and their applications in immuno-labeling and fluorescent imaging of cancer cells, *Langmuir* 26 (2010) 1278–1284.
- [21] Y. Cheng, R.Q. Tan, W.Y. Wang, Y.Q. Guo, P. Cui, W.Y. Song, Controllable synthesis and magnetic properties of Fe<sub>3</sub>O<sub>4</sub> and Fe<sub>3</sub>O<sub>4</sub>@SiO<sub>2</sub> microspheres, *J. Mater. Sci.* 45 (2010) 5347–5352.
- [22] R.Y. Hong, S.Z. Zhang, Y.P. Han, H.Z. Li, J. Ding, Y. Zheng, Preparation, characterization and application of bilayer surfactant-stabilized ferrofluids, *Powder Technol.* 170 (2006) 1–11.
- [23] S.H. Xuan, F. Wang, J.M.Y. Lai, K.Y. Sham, Y.X.J. Wang, S.F. Lee, J.C. Yu, C.H.K. Cheng, K.C.F. Leung, Synthesis of biocompatible, mesoporous Fe<sub>3</sub>O<sub>4</sub> nano/microspheres with large surface area for magnetic resonance imaging and therapeutic applications, *ACS Appl. Mater. Interfaces* 3 (2011) 237–240.
- [24] J. Sun, S.B. Zhou, P. Hou, Y. Yang, J. Weng, X.H. Li, M.Y. Li, Synthesis and characterization of biocompatible Fe<sub>3</sub>O<sub>4</sub> nanoparticles, *J. Biomed. Mater. Res.* 80A (2007) 333–341.
- [25] L.L. Yang, Q.X. Zhao, M. Willander, X.J. Liu, M. Fahlman, J.H. Yang, Effective suppression of surface recombination in ZnO nanorods arrays during the growth process, *Cryst. Growth Des.* 10 (2010) 1904–1910.
- [26] M.H. Chen, Y.N. Kim, C.C. Li, S.O. Cho, Preparation and characterization of magnetic nanoparticles and their silica egg-yolk-like nanostructures: a prospective multifunctional nanostructure platform, *J. Phys. Chem. C* 112 (2008) 6710–6716.
- [27] Z.C. Guo, C.L. Shao, M.Y. Zhang, J.B. Mu, Z.Y. Zhang, P. Zhang, B. Chen, Y.C. Liu, Dandelion-like Fe<sub>3</sub>O<sub>4</sub>@CuTPc hierarchical nanostructures as a magnetically separable visible-light photocatalyst, *J. Mater. Chem.* 21 (2011) 12083–12088.
- [28] X. Liu, X. Chen, Y.F. Li, X.Y. Wang, X.M. Peng, W.W. Zhu, Preparation of superparamagnetic Fe<sub>3</sub>O<sub>4</sub>@alginate/chitosan nanospheres for candida rugosa lipase immobilization and utilization of layer-by-layer assembly to enhance the stability of immobilized lipase, *ACS Appl. Mater. Interfaces* 4 (2012) 5169–5178.
- [29] D.H. Han, J.P. Wang, H.L. Luo, Crystallite size effect on saturation magnetization of fine ferrimagnetic particles, *J. Magn. Magn. Mater.* 136 (1994) 176–182.
- [30] C.R. Lin, Y.M. Chu, S.C. Wang, Magnetic properties of magnetite nanoparticles prepared by mechanochemical reaction, *Mater. Lett.* 60 (2006) 447–450.
- [31] T. Fan, D.K. Pan, H. Zhang, Study on formation mechanism by monitoring the morpholog and structure evolution of nearly monodispersed Fe<sub>3</sub>O<sub>4</sub> submicroparticles with controlled particle sizes, *Ind. Eng. Chem. Res.* 50 (2011) 9009–9018.
- [32] H.H. Jiang, X.Y. Han, Z.L. Li, X.C. Chen, Y.H. Hou, L.G. Gai, D.C. Li, X.R. Lu, T.L. Fu, Superparamagnetic core-shell structured microspheres carrying carboxyl groups as adsorbents for purification of genomic DNA, *Colloids Surf. A: Physicochem. Eng. Aspects* 401 (2012) 74–80.
- [33] G.K. Pradhan, K.M. Parida, Fabrication, growth mechanism, and characterization of α-Fe<sub>2</sub>O<sub>3</sub> nanorods, *ACS Appl. Mater. Interfaces* 3 (2011) 317–323.
- [34] J. Ren, H.Y. Hong, T.B. Ren, X.R. Teng, Preparation and characterization of magnetic PLA-PEG composite particles, *Mater. Lett.* 59 (2005) 2655–2658.
- [35] H.B. Hu, Z.H. Wang, L. Pan, S.P. Zhao, S.Y. Zhu, Ag-coated Fe<sub>3</sub>O<sub>4</sub>@SiO<sub>2</sub> three-ply composite microspheres: synthesis, characterization, and application in detecting melamine with their surface-enhanced Raman scattering, *J. Phys. Chem. C* 114 (2010) 7738–7742.